A Highly Destabilizing Mutation, G37A, of the Bovine Pancreatic Trypsin Inhibitor Retains the Average Native Conformation but Greatly Increases Local Flexibility†

John L. Battiste,‡ Renhao Li,§ and Clare Woodward*

Department of Biochemistry, Molecular Biology, and Biophysics, University of Minnesota, 1479 Gortner Avenue, St. Paul, Minnesota 55108

Received August 21, 2001; Revised Manuscript Received November 27, 2001

ABSTRACT: A point mutation, G37A, on the surface of bovine pancreatic trypsin inhibitor (BPTI) destabilizes the protein by ∼5 kcal/mol, which is very high for addition of one methyl group. In wild-type (WT) BPTI, Gly 37 HN is in an unusual NH−aromatic−NH network of interactions with the ring of Tyr 35 and the side chain HN of Asn 44. G37A was designed to disrupt this interaction, since the ϕ and ψ backbone angles of G37 are not favorable for an amino acid containing a β-carbon. Investigations of the structure and dynamics by NMR methods show that G37A retains the average WT structure. The NH−aromatic−NH interactions remain intact, as indicated by NOEs and the large upfield ring current shift (∼4 ppm) of A37 HN. The NMR structure, confirmed by molecular modeling calculations, requires ϕ and ψ backbone angles that are highly destabilizing when alanine is in position 37. Although the average structure is essentially unchanged, the dynamics are altered dramatically. Many residues in the region of the mutation have increased flexibility, as probed by aromatic ring flip rates and native state hydrogen exchange. We conclude that a large fraction of the destabilization arises from maintaining A37 in a high-energy conformation. This suggests that disruption of the NH−aromatic−NH network is energetically very costly, and may involve other cooperatively linked interactions. The results illustrate the importance of the Gly-Gly sequence at positions 36 and 37 and the 37 HN−35 aromatic interaction to the stability, folding, and dynamics of the BPTI.

Bovine pancreatic trypsin inhibitor (BPTI)[1] is organized around a central β-sheet core capped by N- and C-terminal helices that participate in two buried disulfide bonds (C5−C55 and C30−C51). The protease binding site resides on overlapping loops connected by a solvent-exposed disulfide bond (C14−C38). The fold (Kunitz domain) occurs in a wide variety of mammalian proteins, including a human Alzheimer amyloid precursor. A number of BPTI mutations have been studied for their effect on structure, dynamics, and stability (*1*−*4*), on disulfide-linked folding (*5*−*9*), and on folding of the disulfide-intact BPTI (*10*). High-resolution crystal structures of core mutations F22A, Y23A, N43G, and F45A contain crevices at the site of the replacement of the larger side chain with the smaller one (*2*). There is very little rearrangement of surrounding residues, and the loss of thermodynamic stability ($\Delta\Delta G$ in the range of 2−7 kcal/mol) can be reasonably accounted for by the additional surface area exposed to solvent (*4*). In contrast, Y35G, a mutation that perturbs active site loops of residues 11−17 and 35−43, results in large rearrangements in the vicinity of the mutation, increased flexibility, and non-native hydrogen bonds between protein−protein and protein−water sites (*2*, *11*).

G37A, the BPTI variant under study here, is also in the active site loops. The Gly to Ala replacement introduces a large destabilization (*3*). The $\Delta\Delta G$ of ∼5 kcal/mol is extremely high for addition of a single methyl group near the protein surface, and is on the order of $\Delta\Delta G$ for crevice-forming mutations in the core (*3*). The glycine to alanine mutation was designed to perturb an unusual HN−aromatic interaction between the backbone HN of residue 37 and the ring of Y35 (Figure 1); perturbation is expected since G37 has a backbone conformation that is "disallowed" for alanine. The HN−aromatic interaction between G37 and Y35 is electrostatic in nature, with the partial positive dipole of the HN group interacting with the partial negative charge at the ring center. A similar interaction is proposed in packing of arginine and lysine side chains with aromatic rings (*12*). Theoretical estimates suggest that the HN−aromatic interaction can be worth 1−3 kcal/mol in vacuo (*13*, *14*). Since mutation at position 35 in Y35G results in large loop rearrangements, one might expect mutation at position 37 to have similar consequences. However, initial NMR studies of G37A indicate few changes in HN chemical shifts, as compared to Y35G (*3*). No high-resolution crystal structure is published for this mutation. The three-dimensional NMR structure, reported here, is surprisingly close to that of the

† This work was supported by NIH Grant GM26242. J.L.B. was supported by NIH Postdoctoral Fellowship CA73104.

* To whom correspondence should be addressed. Phone: (435) 946-2949. Fax: (435) 946-8251. E-mail: clare@biosci.cbs.umn.edu.

‡ Present address: 3M Corporate Analytical Technology Center, 3M Center, Building 201-BS-05, St. Paul, MN 55144.

§ Present address: Department of Biochemistry and Biophysics, University of Pennsylvania, Philadelphia, PA 19104.

[1] Abbreviations: BPTI, bovine pancreatic trypsin inhibitor; WT, wild type; NMR, nuclear magnetic resonance; NOE, nuclear Overhauser effect; DQF-COSY, double-quantum-filtered correlated spectroscopy; TOCSY, total correlated spectroscopy; NOESY, nuclear Overhauser effect spectroscopy.

10.1021/bi011693e CCC: $22.00
Published on Web 01/19/2002

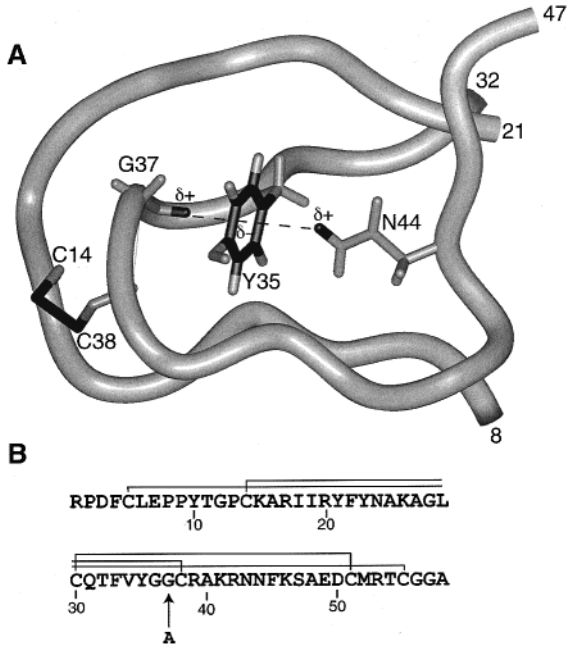

FIGURE 1: Aromatic−NH interactions involving Y35. (A) The backbone of BPTI (5PTI) is shown in gray for the overlapping loops comprising the trypsin binding site. For Y35, G37, and N44, all atoms are shown; those involved in the HN−aromatic−HN interaction are black. The C14−C38 disulfide bond is also black. (B) Sequence of WT BPTI. The position of mutation G37A is marked with an arrow. C5−C55, C14−C38, and C30−C51 disulfide bonds are indicated.

wild type (WT), and the HN−aromatic interaction is, on average, intact. The alanine at position 37 is in a highly strained backbone conformation, and this likely accounts for the large destabilization arising from the mutation. The strain is apparently relieved somewhat by increased flexibility around the mutation site, as indicated by marked increases in the rates of amide proton−deuterium exchange and aromatic ring flips.

MATERIALS AND METHODS

Sample Preparation. The WT and G37A BPTI were overexpressed in *Escherichia coli* and purified as described previously (*2*). The purified protein was dialyzed against H_2O, lyophilized, and stored at −20 °C until it was used. For NMR experiments in H_2O, the lyophilized protein was dissolved in a 90% H_2O/10% D_2O mixture and adjusted to pH 4.6 with HCl. For NMR experiments in D_2O, the lyophilized protein was dissolved in 99.96% D_2O, adjusted to pH 6.5 with DCl. To fully exchange all amide protons with deuterium, WT or G37A was incubated at pH 6.5 overnight (12−16 h) at 70 or 55 °C, respectively. The protein was then lyophilized, resuspended in 99.996% D_2O, and adjusted to pH 4.6 with DCl (nonadjusted pH meter reading). For experiments designed to quantify the rate of amide exchange (H−D), the lyophilized protein (previously at pH 4.6) was dissolved in 99.96% D_2O equilibrated at 4 °C and pH ∼4.0 (low pH and temperature to prevent rapid exchange during the dead time). The sample was quickly adjusted to pH 4.6 and placed in the magnet at 10 °C. The total dead time was ∼10 min. NMR experiments were carried out at multiple time points as described below.

NMR Experiments. The NMR resonances of G37A were assigned through a series of two-dimensional homonuclear NMR experiments (DQF-COSY, TOCSY, and NOESY) in both D_2O and H_2O at 30 °C [WATERGATE solvent suppression (*15*) was used for TOCSY and NOESY experiments in H_2O]. For a detailed comparison, identical spectra were acquired for WT BPTI, rather than relying on previously published chemical shift or NOE data. Assignments were aided by natural abundance ^{13}C HSQC spectra at 30 °C. Distance restraints for modeling calculations were obtained from NOESY spectra at 800 MHz in both H_2O and D_2O with mixing times of 40 ms. NOESY spectra at 10 °C were used to obtain distance restraints for aromatic protons whose ring flips are in intermediate exchange at 30 °C (F45 and Y23 for WT and F45, Y35, and Y23 for G37A). Spectra were processed with the program nmrPipe (*16*) and analyzed with the program XEASY (*17*).

Ring flip rates were measured from two-dimensional (2D) pure exchange experiments (*18*) at 10 °C for WT and G37A. Chemical exchange cross-peaks are exclusively observed in this two-dimensional NOESY-type experiment by alternating the magnetization between the *z*-axis and *xy*-plane in such a way that ROE and NOE cross-relaxation pathways interfere and cancel. Cross-peak volumes were measured at multiple mixing times and fit to the following equation to determine rate constants for flipping of the aromatic ring

$$I(t) = A - 0.5A[1 + \exp(-2kt)] \qquad (1)$$

where $I(t)$ is the cross-peak intensity at mixing time t, A is the intensity of the diagonal peak at time zero, k is the rate constant for chemical exchange, and t is the mixing time. Since ring flipping is reversible, this equation represents the rate of approach to equilibrium (where $k_{for} = k_{rev}$, or $2k$).

Hydrogen exchange rate constants were measured at pH 4.6 and 10 °C on 5 mM WT and G37A protein samples in 99.96% D_2O. For each time point, a 2D TOCSY experiment was acquired with one scan per increment and 128 t_1 increments for a total acquisition time of 8 min. Spectra were acquired in 10 min intervals for ∼1 h, followed by exponentially increasing intervals up to 8 h. At the larger intervals, the TOCSY experiments saw increases to 256 increments with 16 scans (acquisition time of ∼5 h). Exchange was monitored for ∼3 days. The exchange rate for G37 in WT (previously undetermined) was measured at 30 °C with 2 h TOCSY experiments for 1 day. The decays of cross-peak intensities (normalized to a nonexchangeable cross-peak) were fit to a single-exponential equation using the program NMRView (*19*).

Molecular Modeling Calculations. Structures of G37A and WT were calculated using simulated annealing molecular dynamics protocols with the program XPLOR (*20*). Distance restraints from NOESY spectra were treated using r^{-6} summation with no pseudoatom corrections (*21*). Previous stereospecific assignments and torsion angle restraints from WT BPTI (*22*, *23*) were used for G37A if (1) chemical shifts were similar ($\Delta\delta < 0.1$ ppm), (2) qualitative coupling constants from DQF-COSY and the intensity of cross-peaks in TOCSY experiments were similar, and (3) intensities of sequential NOEs were similar. Fifty structures were calculated starting from extended coil protein structures with random ϕ and ψ angles. Convergence of the resulting structures was evaluated via a lack of NOE (>0.5 Å) or dihedral angle (>5.0°) restraint violations.

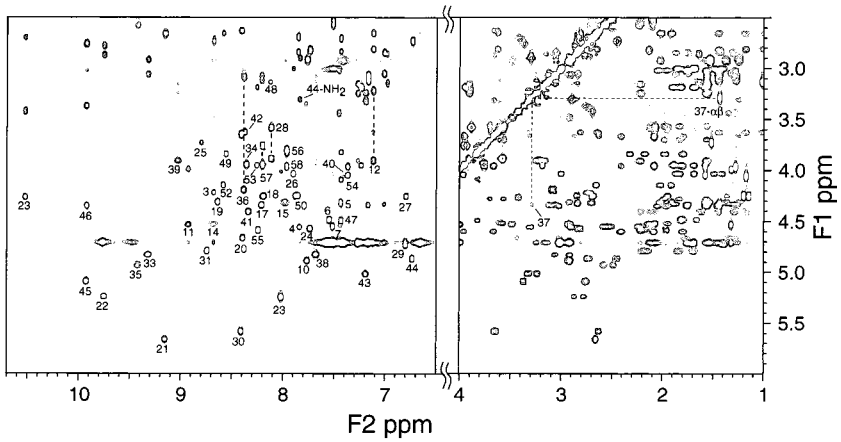

FIGURE 2: 2D TOCSY spectra of G37A. HN−HA cross-peaks are numbered. The two HA peaks for each glycine are connected by a thick dashed line. The cross-peak for A37 HN at 4.32 ppm is bleached in the F2 dimension due to water suppression. The symmetric cross-peak with the HA proton at 3.25 ppm is shown along with connectivity to the HA−HB cross-peaks (thin dashed line). Spectra were obtained with 2.5 mM protein samples in 90% H_2O at 30 °C with a mixing time of 45 ms.

The resulting structures were refined using ^{1}H chemical shifts directly as modeling restraints (*24*). All assigned ^{1}H chemical shifts, except those of aromatic ring protons, were used for refinement calculations. Exchangeable amide protons were included, since the key chemical shift data for BPTI are the ~4 ppm upfield shifts of residue 37 HN and N44 H_δ protons. Chemical shifts of exchangeable protons are very sensitive to temperature and pH; therefore, the random coil chemical shift library was modified to match the pH and temperature conditions used for this study (pH 4.5 and 30 °C) by using temperature coefficient data from the GGXGG peptide series (*25*). The error bounds for exchangeable protons were increased such that any calculated chemical shift within 0.6 ppm of the observed value was not given an energetic penalty in the modeling calculations. This bound was 0.3 ppm for the aliphatic protons. Convergence of the resulting structures was evaluated as described above.

Average structures were generated after superposition of the backbone coordinates for residues 2−55. The average structures were regularized by 1000 steps of energy minimization.

RESULTS

Assignment of G37A and Comparison to WT. A preliminary summary of these results is included in a recent review of our work (*26*). NMR spectra of G37A were assigned via standard 2D techniques (DQF-COSY, TOCSY, and NOESY), by natural abundance ^{13}C HSQC, and by comparison to WT chemical shifts. Figure 2 shows the amide−alpha region of a TOCSY spectrum of G37A in 90% H_2O. Amide proton chemical shifts are very similar to those of the wild type, with the largest amide chemical shift changes being for A16 and G36 (Figure 3). A16 HN was previously misassigned to A40 HN (*3*). Significantly, A37 HN in G37A has little perturbation from WT which has an unusual upfield chemical shift of ~4.3 ppm (*27*). This resonance has not been previously assigned in G37A, and improved water suppression techniques aided in observation of this and other cross-peaks close to the water resonance. Assignment of A37 HN is confirmed by disappearance of the cross-peak after dissolution in D_2O and by the carbon chemical shifts of the

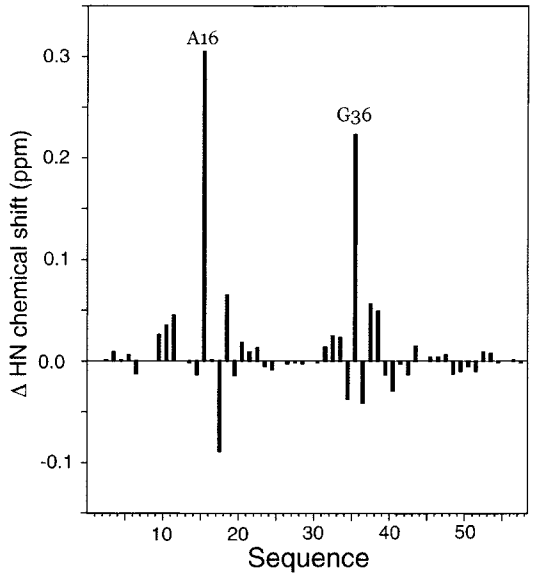

FIGURE 3: Chemical shift difference (G37A − WT) of backbone amide protons of the BPTI. Differences of >0.1 ppm are labeled.

α- and β-carbons that have ^{1}H−^{1}H correlations to A37 HN in the TOCSY spectrum (consistent with an alanine residue; see Figure 2). The magnitude of the upfield chemical shift suggests that the HN−aromatic interaction is intact with the A37 amide proton close to, and centered on, the Y35 ring. Almost all NOEs assigned for G37A are observed in WT or are compatible with A37 Cβ occupying the same position as G37 HA2 in WT (Table 1).

Chemical shifts are sensitive to the fine details of the structural environment such that small changes in atomic coordinates may have measurable effects not detected by NOE analysis. In addition to the amide chemical shift changes shown in Figure 3, a comparison of WT and G37A ^{13}C HSQC spectra is shown in Figure 4. The majority of the protein, including the central hydrophobic core around the β-sheet, has identical chemical shifts for equivalent atoms in WT and G37A. Small but measurable effects are observed for residues 11−19 and 32−38 in the two overlapping loops extending slightly into the β-sheet. Moderate changes are observed for only residues 14−18 and 34−38 in the region immediately adjacent to the mutation. The two largest

Table 1: NOEs Involving Residue 37 in WT and G37A

WT		G37A	
position 37	other atom in NOE	position 37	other atom in NOE
HN	Y35 HD1	HN	Y35 HD1
	Y35 HE2		Y35 HE2
	Y35 HE1		—[a]
	C38 HN		C38 HN
HA1	A16 HB[b]	HA	A16 HB[b]
	I18 HD1[b]		I18 HD1[b]
	Y35 HD2		Y35 HD2
	Y35 HE2		Y35 HE2
	C38 HN		C38 HN
HA2	A16 HB[b]	HB[b]	—[a]
	—[a]		A16 HN
	I18 HD1[b]		I18 HD1[b]
	Y35 HE2		Y35 HE2
	C38 HN		C38 HN

[a] NOE not observed or has spectral overlap. [b] Methyl group of three hydrogens.

Table 2: Structural Statistics for NOE-Based and Chemical Shift-Refined BPTI Structures[a]

	rms deviation			
	NOE-based G37A (32)	CS-refined G37A (23)[b]	NOE-based WT (30)	CS-refined WT (26)[b]
NOE (Å)[c]	0.0195	0.0202	0.0311	0.0334
dihedral (deg)[d]	0.365	0.408	0.283	0.390
chemical shift (ppm)	0.533[e]	0.371	0.470[e]	0.369
bonds (Å)	0.00200	0.00198	0.00256	0.00272
angles (deg)	0.552	0.555	0.580	0.588
impropers (deg)	0.369	0.396	0.385	0.423
backbone (Å)[f]	0.442	0.407	0.411	0.379
heavy chain (Å)[f]	0.975	0.959	1.014	0.979

[a] rms deviations were calculated for the entire family of converged structures (number per 50 calculated given in parentheses) and averaged. [b] Structures refined directly using ^{1}H chemical shifts. [c] No violations of >0.5 Å in any structure. [d] No violations of >5° in any structure. [e] Chemcial shift not included in the target function for these structures. [f] For residues 2−55.

changes in the methyl region are A16 HB and I18 HD1, both of which have NOEs to the A37 methyl group. Static introduction (no conformational change upon mutation) of a methyl group into the crystal structure of WT places it in van der Waals contact with the methyl groups of A16 and I18. Overall, the chemical shift changes and the NOE analysis suggest small or no changes in the conformation of G37A relative to that of WT.

Structure Calculations. The similarity of the G37A structure to WT is surprising, since this requires that A37 have ϕ and ψ angles close to the crystal structure values of 105° and −7°, respectively, which are highly unfavorable for a non-glycine amino acid. To examine more rigorously whether A37 adopts a backbone conformation similar to that of WT, families of low-energy structures were determined from simulated annealing molecular dynamics calculations (XPLOR program) using distance and torsion restraints from NOEs and *J* couplings, respectively (Table 2). The resulting structures (hereafter termed "NOE-based" structures) of both WT and G37A are very similar. Localized differences are observed for residue 37 with ϕ and ψ angles of 180° and −30° and 80° and −10° in G37A and WT, respectively. In G37A, the A37 HN bond vector is parallel to the ring plane of Y35 rather than perpendicular (magenta in Figure 5). The parallel orientation is inconsistent with the chemical shift

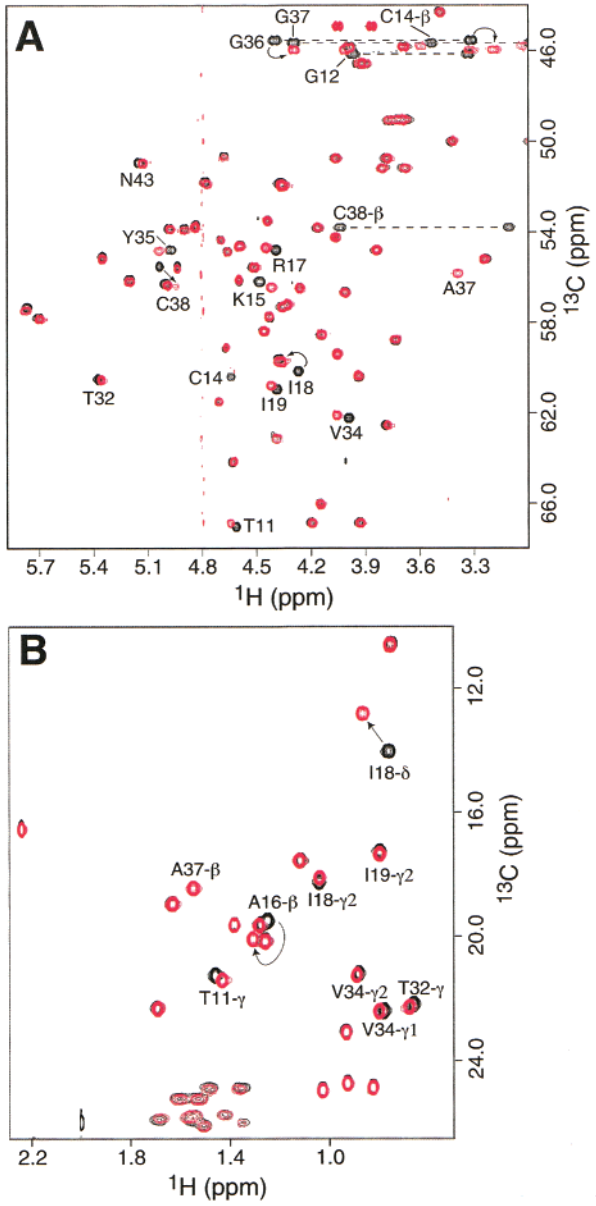

FIGURE 4: Overlaid ^{13}C HSQC spectra of WT and G37A. (A) α or (B) methyl region of HSQC with G37A in red and WT in black. Cross-peaks with detectable changes upon mutation are labeled. Methylene protons (Gly α or Cys β) bonded to the same carbon are connected by dashed lines. For both WT and G37A spectra, the protein concentration was 5 mM.

data, since the HN atom is too far away from the ring of Y35 to result in an ~4 ppm upfield shift. Further, the NOEs between A37 HN and Y35 ring protons have small violations of ~0.2 Å. A likely explanation for the inconsistencies in the NOE-based structures is that the force field used in XPLOR has large energetic penalties for placing an alanine residue in the WT ϕ and ψ conformation, where there would be vdw overlap between A37 methyl protons and the carbonyl oxygen of G36. The energetic penalty for slightly violating the two A37 HN−Y35 ring NOEs is probably smaller than the vdw penalty, and it appears that modeling based solely on NOEs and *J* couplings may be insufficient to determine the structure in this region.

Modeling experiments were performed to test the hypothesis that the commonly used suite of penalties in the force field results in inaccuracies in the NOE-based structure of

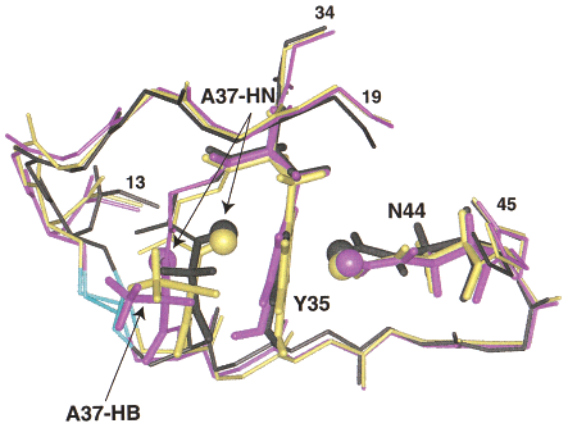

FIGURE 5: Average structures from molecular dynamics calculations of G37A and WT. G37A with (yellow) and without (magenta) chemical shift refinement are superimposed on WT (black). Loops of residues 13−19 and 34−45 are displayed. Only backbone atoms are shown except for side chains of Y35, A37, and N44 (thick sticks), and for the disulfide of residues 14 and 38 (cyan). HN protons involved in NH−aromatic−NH interaction are CPK spheres. Arrows mark the positions of A37 HN and CB. In the text, the magenta structure is termed NOE-based and the yellow structure is termed CS-refined.

G37A, especially in the region of the mutation. While the NOE data sets of WT and G37A are very similar, they are not identical. To examine whether differences between WT and G37A arise from the NOE data sets, the distance restraints for G37A were used to calculate structures of WT. NOEs to the methyl protons of A37 were translated to the G37 HA2 proton by adding a correction to the upper bound of 1.0 Å. The structures of WT obtained with the G37A NOE data set were nearly identical to those obtained with WT NOE data set (data not shown). Importantly, the HN proton of G37 in these calculations is orientated in the center of the Y35 ring, as in the crystal structure. In a separate modeling experiment, the ϕ and ψ torsion angles of A37 were restrained to within 30° of the crystal structure values; the outcome is that the structures of G37A converge with few NOE violations, indicating that the nativelike structure is consistent with the NOE data for G37A. Further, the vdw energy terms are ~5−10 kcal/mol higher on average than those of structures calculated with the A37 ϕ and ψ values unrestrained, suggesting that WT-like ϕ and ψ angles for residue 37 result in a high-energy conformation in G37A that is selected against during refinement (in the absence of sufficient NMR restraints). Overall, we conclude that the force field is the major factor contributing to the local differences in the backbone conformation between WT and the NOE-based structure of G37A.

Refinement of G37A Structure with Chemical Shifts. The major piece of evidence contradicting the NOE-based structure of G37A is the chemical shift of A37 HN. Semiempirical methods for calculating chemical shifts from three-dimensional structures of proteins are reasonably predictive of observed chemical shift values (*28*, *29*). In particular, the contribution of aromatic ring currents to chemical shift is well-characterized. Two available implementations were used to calculate the chemical shift of A37 HN in the initial NOE-based structure of G37A [program of Williamson et al. (*29*) and XPLOR (*20*, *24*)]. Both programs give values of ~8 ppm, almost 4 ppm away from

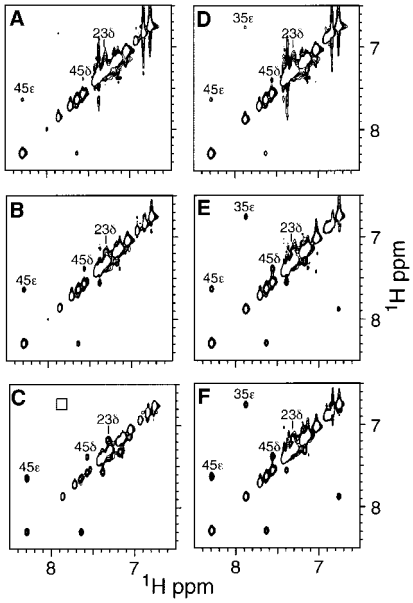

FIGURE 6: 2D pure exchange spectroscopy of WT and G37A. Exchange spectra at mixing times of 4, 8, and 100 ms for WT (A−C, respectively) and 4, 8, and 16 ms for G37A (D−F, respectively). Assignment of the aromatic ring proton in exchange ("flip") is indicated. Y35 δ- and Y23 ϵ-protons are too close to the diagonal to be resolved. The box in panel C shows the position where a Y35 ϵ-cross-peak would arise.

the observed value of 4.32 ppm. Similar calculations on the crystal or NMR structure of WT give values around 6 and 5 ppm, respectively. While highly precise calculations of the chemical shift from structure are still not feasible, such a large deviation (~4 ppm) between the calculated and experimental chemical shift suggests a structural inaccuracy associated with using only distance and torsion restraints in this case.

Recent advances in using chemical shifts directly in structure determination (*24*, *30*) make it possible to use ^{1}H chemical shift information of G37A for structural refinement. The majority of the chemical shift (CS)-refined structures converge with no NOE violations of >0.5 Å or dihedral angles of >5° (Table 2). The average structures of G37A, with and without CS refinement, are very similar (backbone rmsd of 0.48 Å) except for the region right around A37 (Figure 5). The backbone of A37 reorients to position the HN in the center of the Y35 ring (to satisfy the large upfield chemical shift), resulting in a backbone conformation that is very similar to WT (Figure 5). The ϕ and ψ angles for A37 in the family of CS-refined structures are 72.0 ± 4.0° and −0.7 ± 10.2°, respectively, compared to 99.0 ± 3.9° and −34.2 ± 8.1°, respectively, in the WT NMR structure (also with CS refinement), and 104.9° and −7.4°, respectively, in the crystal structure. Despite the small differences between these structures, it is clear that the backbone of A37 is in an unfavorable conformation.

Aromatic Ring Flip Rates of G37A. The effect of the G37A mutation on protein dynamics is reflected in aromatic ring flip rates which probe motions on slower time scales (*31*, *32*). The symmetric protons at positions d and e of three aromatic rings in the BPTI (Y23, Y35, and F45) are in slow chemical exchange, and their flip rates were measured directly by a pure 2D exchange spectroscopy experiment (*18*). Figure 6 shows the buildup of exchange cross-peaks

Table 3: Aromatic Ring Flip Rates (s^{-1}) at 10 °C and pH 4.6

residue	WT	G37A
Y23	4	6
Y35	<0.3	40
F45	57	56

at 10 °C for WT and G37A. In G37A, the rate of buildup is roughly similar for all three slowly flipping rings. In WT, Y35 flips very slowly, with no detectable exchange even after a mixing time of 100 ms, and only an upper limit can be put on its flip rate (Table 3). Nevertheless, it is at least 2 orders of magnitude slower than Y35 in G37A, indicating that the region immediately surrounding the site of mutation has an increased level of internal motions.

H−D Exchange in G37A. Another probe of local dynamics in proteins is hydrogen isotope exchange. While global unfolding can lead to hydrogen exchange, under common experimental conditions many amide protons exchange at a rate faster than the unfolding rate, presumably through local motions of the folded state that expose buried groups to solvent and/or that allow solvent to penetrate the protein interior (*33*, *34*). Under these conditions, the relative rate of H−D exchange for various amide groups is a qualitative probe of the internal dynamics of the folded state.

Earlier H−D exchange data provided initial evidence for increased flexibility in G37A (*3*). However, many HN groups in the loops connected by the disulfide bond between residues 14 and 38 have fast HN exchange rates, and were not previously detected for G37A. In addition, amide H−D exchange rates for position 37 have not heretofore been measured for either WT or G37A. A complete set of H−D exchange rates at a lower temperature (10 °C) were obtained by using very short phase sensitive TOCSY experiments (∼10 min) to improve the resolution of detectable peaks during the initial stages of H−D exchange. The values of all measured exchange rates for WT and G37A are given in Table 4. Most values for the very slowly exchanging protons were not determined here at 10 °C, but extrapolated from previously measured values at 30 °C for both WT and G37A (*3*). The one exception was position 37 in WT, for which no value has previously been measured. The value of this amide in WT was measured at 30 °C and pH 4.5 and extrapolated to 10 °C using an estimated activation energy of 30 kcal/mol. In Figure 7, the amide exchange rate constants of G37A residues are plotted against the rate constants of the same amide in WT. The hydrogen exchange data fully explain the decreased $\Delta G°$ for G37A. As described previously (e.g., in refs *3* and *34*), the very slowest exchanging amides in BPTI exchange only by an *unfolding* mechanism and their appearance on the dotted line of Figure 7 is in agreement with a $\Delta\Delta G°$ of 5 kcal/mol. The other amides exchange primarily by a mechanism that involves motions of the *folded* state. Among these, most exchange with the same rate in WT and the mutant, in keeping with extensive exchange data (*3*), and these are shown as white triangles along the diagonal in Figure 7. However, a group of 11 amides in G37A exchange by the folded state mechanism with rates at least an order of magnitude faster than in WT [Figure 7 (▲)], and their proximity to the mutation site is clear [Figure 8 (white dot vdw spheres)]. The mutation-affected region includes the two overlapping loops connected by the disulfide bond between residues 14 and 38 and the β-bridge from residues 10−18 and 35−45. The conclusion is that the Gly to Ala replacement affects fluctuations of the folded state only in the region of the mutation, and not throughout the entire molecule.

Table 4: Hydrogen Exchange Rates (min^{-1}) of WT and G37A at 10 °C and pH 4.6

residue number	WT	G37A	residue number	WT	G37A
5	5.1×10^{-5}	$9 \times 10^{-5\,b}$	32	1.4×10^{-3}	7.7×10^{-4}
6	$4 \times 10^{-5\,b}$	$2 \times 10^{-5\,b}$	33	$1 \times 10^{-7\,b}$	$6 \times 10^{-7\,a}$
7	$2 \times 10^{-5\,b}$	$2 \times 10^{-5\,b}$	34	1.6×10^{-3}	2.0×10^{-3}
10	1.3×10^{-4}	1.0×10^{-3}	35	$3 \times 10^{-7\,b}$	3.2×10^{-4}
12	8.0×10^{-3}	6.0×10^{-3}	36	$1 \times 10^{-5\,b}$	8.2×10^{-4}
14	1.6×10^{-4}	1.8×10^{-2}	37	$3 \times 10^{-6\,d}$	2.0×10^{-3}
16	1.9×10^{-4}	4.3×10^{-3}	38	7.0×10^{-3}	2.6×10^{-3}
17	5.0×10^{-2}	3.8×10^{-2}	41	$7 \times 10^{-5\,b}$	4.9×10^{-3}
18	$8 \times 10^{-8\,b}$	1.3×10^{-4}	42	4.2×10^{-2}	1.0×10^{-2}
19	4.4×10^{-3}	2.3×10^{-3}	43	2.6×10^{-3}	4.4×10^{-3}
20	$1 \times 10^{-8\,b}$	$2 \times 10^{-7\,a}$	44	$3 \times 10^{-7\,b}$	$8 \times 10^{-5\,b}$
21	$2 \times 10^{-12\,c}$	$4 \times 10^{-7\,a}$	44_{side}	$1 \times 10^{-5\,e}$	1.5×10^{-4}
22	$2 \times 10^{-12\,c}$	$2 \times 10^{-7\,a}$	45	$1 \times 10^{-7\,b}$	$8 \times 10^{-6\,b}$
23	$2 \times 10^{-12\,c}$	$8 \times 10^{-8\,a}$	47	3.1×10^{-3}	3.9×10^{-3}
24	$1 \times 10^{-7\,b}$	$2 \times 10^{-7\,a}$	48	4.0×10^{-2}	2.2×10^{-2}
25	1.6×10^{-2}	1.0×10^{-2}	51	$8 \times 10^{-6\,b}$	$9 \times 10^{-6\,b}$
27	2.9×10^{-3}	3.7×10^{-3}	52	$4 \times 10^{-6\,b}$	$5 \times 10^{-6\,b}$
28	2.8×10^{-4}	3.9×10^{-4}	53	$8 \times 10^{-6\,b}$	$5 \times 10^{-6\,b}$
29	$5 \times 10^{-7\,b}$	$2 \times 10^{-7\,a}$	54	7.4×10^{-5}	8.1×10^{-5}
30	6.5×10^{-3}	5.2×10^{-3}	55	$3 \times 10^{-6\,b}$	$6 \times 10^{-6\,b}$
31	$8 \times 10^{-8\,b}$	$8 \times 10^{-8\,a}$	56	1.1×10^{-4}	2.0×10^{-4}

[a] Estimated by extrapolation from values obtained at pH 3.5 and 30 °C using an activation energy of 23−37 kcal/mol as calculated from two values between 30 and 40 °C (*43*). [b] Estimated by extrapolation from values obtained at pH 3.5 and 30 °C using an activation energy of 35 kcal/mol. [c] Estimated by extrapolation from values obtained at pH 3.5 and 30 °C using an activation energy of 78 kcal/mol. Exchange rates for WT and G37A at pH 3.5 and 30 °C are reported in ref *3*. [d] Extrapolated from pH 4.5 and 30 °C using an activation energy of 30 kcal/mol. [e] Extrapolated from pH 4.5 and 25 °C (reported for WT in ref *44*) using an activation energy of 30 kcal/mol.

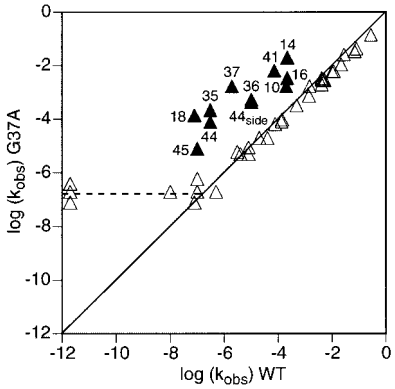

FIGURE 7: Plot of the logarithm of the measured H−D exchange rate constants for WT and G37A. The dashed line indicates protons that exchange by a global unfolding mechanism in G37A. Black triangles indicate protons that exchange 1 order of magnitude faster in G37A [$\log(k_{G73A}/k_{WT}) > 1$]. 44_{side} denotes the secondary amide on the side chain of Asn 44.

Isomerization of the Disulfide Bond between Residues 14 and 38. Conformational exchange broadening was observed for some aliphatic protons in the region of the mutation, particularly for C14 and C38, which are linked in a disulfide bond. At 30 °C, the C14 HA was severely broadened, while the C38 β-protons were completely absent. The variation of chemical shift with temperature for the β-protons of C38 is shown in Table 5. G37A shows more pronounced behavior

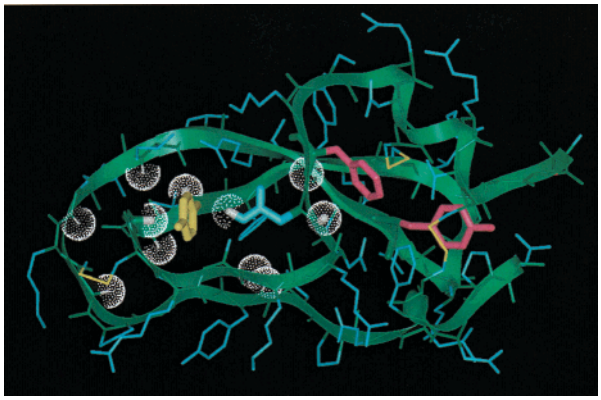

FIGURE 8: Diagram showing the positions of the black triangles in Figure 7 on the tertiary structure of the BPTI. Accelerated amide protons are white vdw dot surfaces. Heavy atoms of aromatic rings listed in Table 3 are yellow and red, indicating increased or no acceleration of the flip rate upon mutation, respectively. Side chain heavy atoms of N44, whose side chain amide proton exchange rate is accelerated upon mutation, are thick cyan sticks. The NH−aromatic−NH backbone (37)−ring (35)−side chain (44) network is apparent in the orientation of the two H atoms with white vdw surfaces on either side of the yellow Y35 ring and pointing to its center.

Table 5: Chemical Shifts of β-Protons of C38 at Different Temperatures

temperature (°C)	WT	G37A
10	3.95/3.01	3.99/3.07[a]
30	3.92/3.00	—[a]
60	3.83/3.04[a]	3.57/3.17

[a] Conformational exchange broadening observed. A dash indicates broadening that was severe enough to prevent observation of cross-peaks.

than WT in conformational exchange broadening and coalescence of these peaks at higher temperatures (i.e., upfield peak moves downfield and vice versa). Similar but more severe broadening behavior was observed for the G36S mutant, which was explained as an isomerization between a minor conformation with the χ_1 angle of C38 rotated 120° (*35*). Corroboration of this hypothesis has been observed in a recently determined crystal structure of the BPTI with mutations in the trypsin binding loop (T11A/P13A/K15R) (*36*). In this crystal structure, electron density is observed for two different conformations of the disulfide bond between residues 14 and 38, which agrees with the NMR analysis. In the case of G36S, the minor conformation was substantial enough (~20% at 4 °C) to observe slow exchange cross-peaks in ROESY and COSY spectra that permit assignment and identification of the alternative C38 isomer (*35*). No such cross-peaks could be obtained for G37A (data not shown) or WT (*35*) at 5 °C, probably indicating a smaller fraction for the minor conformer. Nevertheless, the chemical shift behavior of both WT and G37A is consistent with a rotation of the χ_1 angle of C38, since the β-protons would flip orientation (HB1 becomes the downfield peak and HB2 the upfield peak), resulting in coalescence at higher temperatures (i.e., intermediate to fast exchange). Broadening at lower temperatures and larger changes in chemical shift compared to WT are consistent with an increase in the percentage of the minor conformation in G37A and/or the exchange rate between the conformers.

DISCUSSION

G37A Structure. The accuracy of the NMR structure determined with and without chemical shift refinement is the critical issue for analysis of G37A. Overall, for a protein of this size, NMR structures are of very high quality and comparable to crystal structures; however, G37A appears to be a special case where the presence of a "bad" configuration complicates the calculations. Molecular modeling protocols are designed to disfavor such conformations, and a preponderance of data from NMR or crystallography is needed to override the energetic penalties. In this case, the large 4 ppm chemical shift change (from random coil) of A37 HN provides evidence for an inaccuracy in the structure obtained from standard NOE-based calculations. Ascription of the large chemical shift changes to ring currents requires in this case the proximity of A37 HN to the center of an aromatic ring. Several other protons in BPTI have large chemical shift changes due to ring currents [C5 Hα, N44 H$_\delta$, and P9 Hβ ($\geq$2 ppm)]. Chemical shifts of these protons, in contrast to that of A37 HN, are approximately predicted from NOE-based structures of G37A. While inclusion of chemical shifts directly in molecular modeling calculations is not a standard technique, the use here is a very good test case, since the measured effect is so large. Even with large errors in chemical shift prediction, the CS refinement produces fairly strict requirements on the location of the A37 HN proton.

In addition to ^{1}H chemical shifts used for refinement, ^{13}C chemical shifts can also be employed in a semiquantitative fashion to assess the accuracy of the G37A structure, since protein backbone ^{13}C chemical shifts are primarily a function of the ϕ and ψ angles (*37*, *38*). Chemical shifts for A37 Cα and Cβ of 55.5 and 18.1 ppm are 3.2 and −0.9 ppm different from random coil values, respectively. The average ϕ and ψ angles for A37 in the NOE-based structure of G37A (180° and 22°, respectively) are inconsistent with the observed carbon chemical shifts. Angles of 180° and 22° are expected to produce a slightly negative and positive shift in Cα and Cβ, respectively, the opposite of what is observed (especially the large 3 ppm shift in Cα). In particular, the ϕ angle would require adjustments of at least 40° to approach regions of the $\phi-\psi$ map that are consistent with observed chemical shifts. On the other hand, the ϕ and ψ angles in the CS-refined structure of G37A agree well with the measured ^{13}C chemical shifts. Note that the ^{13}C chemical shifts were not used directly in the refinement protocol, since the available implementation in XPLOR is not well-parametrized over all regions of $\phi-\psi$ space. The potential effect on ^{13}C chemical shifts from ring currents (*39*) is negligible for A37, indicating that the observed chemical shifts should be dominated by the backbone conformation. It is also worth noting that the $^3J_{HNHa}$ coupling constant (standard NMR method for determining ϕ) was not measured for A37 due to the lack of a cross-peak in DQF-COSY spectra. The lack of a cross-peak could be due to a very small coupling constant or conformational exchange broadening (NOESY cross-peaks of A37 HN were broad); therefore, no ϕ torsion restraint for A37 was applied in the modeling calculations. Furthermore, while a small J coupling constant is consistent with the WT ϕ angle, a large range of other angles is also possible (from ~0° to 180°).

In summary, ^{1}H and ^{13}C chemical shift data strongly support a backbone conformation for residue 37 very similar to WT (Figure 5), and the overall structure of G37A appears to be nearly indistinguishable from WT.

Energetic Analysis of the G37A Mutation. Since G37A and WT structures are so similar, it is difficult to attribute a significant fraction of the 5 kcal/mol destabilization (*3*) to disruption of native contacts. As described, the HN−aromatic interaction is intact. Detailed comparison of side chain packing and backbone hydrogen bonds shows only one possible difference, perturbation of the hydrogen bond between A16 HN and G36 CO. In the average structure, the A16 HN−G36 CO distance (4.2 Å heavy atom) is larger than the standard criterion for hydrogen bonding. However, the flexible loop containing A16 has higher rms deviations and is near the surface (fewer NOEs per residue), rendering uncertain the distance calculation as a criterion of hydrogen bonding (many individual structures do meet the criteria for hydrogen bonding). Some rearrangement of A16 is reasonable due to the introduction of the methyl group at position 37. If a methyl group is grafted onto the crystal structure of WT, there is minor vdw overlap between A37 HB and A16 HB and I18 HD1. To accommodate the methyl group, the backbone of the loop surrounding A16 appears to expand a few tenths of an angstrom, and to orient the HN bond vector away from G36. Several parameters for A16 NH change in G37A, suggesting a perturbation of the hydrogen bond. A16 HN has the largest chemical shift change in G37A (∼0.3 ppm), which presumably reflects changes in the electrostatic and anisotropic environment of the G36 carbonyl. A16 amide H−D exchange is accelerated by a factor of 20, although this could be due to increased flexibility rather than weakening or disruption of the hydrogen bond (see below). Last, the A16 HN temperature coefficient (change in chemical shift as a function of temperature) increases by a factor of 2 from −2.2 to −4.6 ppb/K, while all other amide temperature coefficients in G37A are similar to those in WT. The temperature coefficient and H−D exchange data are intermediate between that typically observed for hydrogen bonded and that for non-hydrogen-bonded amides (*40*). Overall, the data point to weakening of the A16 HN−G36 CO hydrogen bond, and probably not complete disruption. The actual energetic cost of this depends on compensating hydrogen bonds with solvent.

The only clearly destabilizing feature in G37A is the strained backbone conformation of A37. Exposure to solvent of the methyl group of Ala37 may also decrease the stability of G37A. Energetic analysis of Ramachandran plots of $\phi-\psi$ space for an alanine residue give estimates of penalties of up to 2−4 kcal/mol for placing A37 in the backbone conformation observed in G37A (*41*). This accounts qualitatively for a major portion of the destabilization of the mutant. Keeping A37 in a high-energy conformation implies that the native backbone structure at residue 37 is critical for maintaining the overall stability because this maintains the HN−aromatic interaction between residues 37 and 35 and/or a network of cooperative interactions which collectively are worth more than 4 kcal/mol of stabilizing free energy difference. Theoretical estimates of the HN−aromatic interaction energy are 1−3 kcal/mol in vacuo (*13*, *14*), significantly lower than that of a standard hydrogen bond. It is likely that a set of cooperative interactions linked to the interaction between residues 37 and 35, rather than only the interaction between residues 37 and 35, are maintained in G37A at the cost of the strained backbone of residues 36 and 37. The set presumably includes the other NH−aromatic interaction of Y35 with the side chain primary amide NH proton of N44, on the other side of the ring (Figure 1). Also included in the set may be the two backbone hydrogen bonds of G36 to T11 and A16, connecting either side of the long active site binding loop to the turn conformation of residues 35−44 leading to the β-bridge. The entropic gain from increased flexibility in the vicinity of the mutation presumably eases the energetic cost of the A37 ϕ and ψ angles.

In summary, the strain in the backbone configuration of residues 36 and 37 of G37A is the most obvious contribution to the ∼5 kcal/mol of decreased global stability. Other contributions may arise from exposure of the methyl group of Ala37 to solvent, and/or from perturbation of the A16 NH−G36 CO hydrogen bond.

Dynamics of G37A. While G37A does not have dramatic alterations in average structure, it does have large motional changes in the region of the mutation. G37A provides an interesting comparison to other BPTI mutants and strengthens the argument for the existence of subdomains with different motional properties (*3*). The slow exchange core (subdomain) of BPTI, as defined by the slowest protons to exchange with D_2O, comprises the central β-sheet and short β-bridge (residues 21−23, 31, 33, and 45). Mutations in this region have large effects on stability, but have minimal effects on local structure or flexibility. F22A, Y23A, N43G, and F45A all produce crevices with little rearrangement of surrounding atoms (*1*). The effects on hydrogen exchange or ring flip rates are highly localized to atoms in direct contact with the mutated side chain (i.e., on the crevice surface in mutant), with little effect on the motional properties in the remainder of the subdomain (*3*). The slow exchange core remains more rigid than the rest of the molecule. On the other hand, Y35G results in large structural rearrangements of the overlapping loop subdomain (*2*) and increases the flexibility of the entire subdomain as measured by ring flips and H−D exchange (*3*), and by ^{15}N-transverse relaxation rates of amide protons (*42*). G37A contrasts with Y35G in not having large structural rearrangements of the backbone, even though it apparently requires a strained conformation.

Although the G37A average structure does not change, while Y35G does (*2*, *42*), both mutations result in an increased level of internal motions over the entire loop subdomain. Rearrangement of the average structure is therefore not the key correlate of increased ring flip or H−D exchange rates; rather, the intrinsic balance of structure and dynamics underlies the increased flexibility of the loop subdomain accompanying destabilization. Maintaining A37 in a strained backbone conformation likely decreases the energy barrier to alternative backbone conformations that favor Y35 ring flips and more rapid H−D exchange. On average, G37A contains the HN−aromatic interaction between residues 37 and 35, but is more likely than WT to fluctuate between other backbone conformations that might disrupt the HN−aromatic interaction or other interactions. This would contribute to destabilization, and would also explain the increased Y35 ring flip rate and increased H−D exchange rates in the absence of changes in average ring packing and in static solvent accessibility.

SUMMARY AND CONCLUSIONS

The NMR structure and dynamics have been characterized for BPTI mutant G37A. In this variant, the amino acid replacement is in the vicinity of active site loops of residues 8−17 and 36−44. Compared to that of WT, the global stability of G37A is lowered by 5 kcal/mol. Such a large destabilization is surprising for addition of one methyl group on the protein surface, and even more so for a mutant in which the average structure essentially can be superimposed on WT. Although the NMR structure of G37A retains the average WT structure, including the unusual NH−aromatic−NH network among residues 37, 35, and 44, the local flexibility of the loop subdomain is significantly increased. Enhanced internal motions of this region are indicated by a higher ring flip rate of Y35 but not of other buried rings, faster rates of folded state hydrogen exchange around the mutation site, and increased isomerization of the interloop disulfide bond between residues 14 and 38.

Some, but not all, of the large global destabilization can be ascribed to the highly unfavorable backbone ϕ and ψ angles of residue 37 when alanine instead of glycine occupies that position. Even in the absence of a discernible change in the average structure, the active site loop region in G37A therefore takes on a higher energy conformation and, in increased local excursions from the average, probably samples conformations in which the level of NH−aromatic−NH network interactions, and other linked interactions, is diminished. The ring flip and hydrogen exchange data demonstrate that the loop region undergoes local motions that are not propagated to the rest of the protein.

These results support the importance of the NH−aromatic interaction between residues 37 and 35 to the stability, dynamics, and folding of BPTI. It appears to be the key to a network of coupled interactions that join the loop region to the protein core. Its perturbation results in a large decrease in global stability, a significant increase in local flexibility of the loop domain, and a kinetic trap in the folding process (*10*).

REFERENCES

1. Danishefsky, A. T., Housset, D., Kim, K. S., Tao, F., Fuchs, J., Woodward, C., and Wlodawer, A. (1993) *Protein Sci. 2*, 577−587.
2. Housset, D., Kim, K. S., Fuchs, J., Woodward, C., and Wlodawer, A. (1991) *J. Mol. Biol. 220*, 757−770.
3. Kim, K. S., Fuchs, J. A., and Woodward, C. K. (1993) *Biochemistry 32*, 9600−9608.
4. Kim, K. S., Tao, F., Fuchs, J., Danishefsky, A. T., Housset, D., Wlodawer, A., and Woodward, C. (1993) *Protein Sci. 2*, 588−596.
5. Goldenberg, D. P. (1988) *Biochemistry 27*, 2481−2489.
6. Goldenberg, D. P., Frieden, R. W., Haack, J. A., and Morrison, T. B. (1989) *Nature 338*, 127−132.
7. Coplen, L. J., Frieden, R. W., and Goldenberg, D. P. (1990) *Proteins 7*, 16−31.
8. Mendoza, J. A., Jarstfer, M. B., and Goldenberg, D. P. (1994) *Biochemistry 33*, 1143−1148.
9. Zhang, J. X., and Goldenberg, D. P. (1997) *Protein Sci. 6*, 1549−1562.
10. Li, R., Battiste, J. L., and Woodward, C. (2002) *Biochemistry 41*, 2246−2253.
11. Beeser, S. A., Goldenberg, D. P., and Oas, T. G. (1997) *J. Mol. Biol. 269*, 154−164.
12. Burley, S. K., and Petsko, G. A. (1986) *FEBS Lett. 203*, 139−143.
13. Levitt, M., and Perutz, M. (1988) *J. Mol. Biol. 201*, 751−754.
14. Cheney, J., Cheney, B. V., and Richards, W. G. (1988) *Biochim. Biophys. Acta 954*, 137−139.
15. Piotto, M., Saudek, V., and Sklenar, V. (1992) *J. Biomol. NMR 2*, 661−665.
16. Delaglio, F., Grzesiek, S., Vuister, G., Zhu, G., Pfeifer, J., and Bax, A. (1995) *J. Biomol. NMR 6*, 277−293.
17. Bartels, C., Xia, T., Billeter, M., Guntert, P., and Wuthrich, K. (1995) *J. Biomol. NMR 6*, 1−10.
18. Fejzo, J., Westler, W. M., Macura, S., and Markley, J. L. (1990) *J. Am. Chem. Soc. 112*, 2574−2577.
19. Johnson, B. A., and Blevins, R. A. (1994) *J. Biomol. NMR 4*, 603−614.
20. Brünger, A. T. (1992) *X-PLOR version 3.1: a system for crystallography and NMR*, Yale University Press, New Haven, CT.
21. Fletcher, C. M., Jones, D. M. N., Diamond, R., and Neuhaus, D. (1996) *J. Biomol. NMR 8*, 292−310.
22. Wagner, G., Braun, W., Havel, T. F., Schaumann, T., Go, N., and Wuthrich, K. (1987) *J. Mol. Biol. 196*, 611−639.
23. Berndt, K. D., Guntert, P., Orbons, L. P. M., and Wuthrich, K. (1992) *J. Mol. Biol. 227*, 757−775.
24. Kuszewski, J., Gronenborn, A. M., and Clore, G. M. (1995) *J. Magn. Reson., Ser. B 107*, 293−297.
25. Merutka, G., Dyson, H. J., and Wright, P. E. (1995) *J. Biomol. NMR 5*, 14−24.
26. Woodward, C., Barbar, E., Carulla, N., Battiste, J., and Barany, G. (2001) *J. Mol. Graphics Modell. 19*, 94−101.
27. Tüchsen, E., and Woodward, C. (1987) *Biochemistry 26*, 1918−1925.
28. Osapay, K., and Case, D. A. (1991) *J. Am. Chem. Soc. 113*, 9436−9444.
29. Williamson, M. P., Asakura, T., Nakamura, E., and Demura, M. (1992) *J. Biomol. NMR 2*, 83−98.
30. Clore, G. M., and Gronenborn, A. M. (1998) *Proc. Natl. Acad. Sci. U.S.A. 95*, 5891−5898.
31. Wagner, G., and Wuthrich, K. (1978) *Nature 275*, 247−248.
32. Wuthrich, K., and Wagner, G. (1978) *Trends Biochem. Sci. 3*, 227−230.
33. Woodward, C. K., Simon, I., and Tuchsen, E. (1982) *Mol. Cell. Biochem. 48*, 135−160.
34. Li, R., and Woodward, C. (1999) *Protein Sci. 8*, 1571−1590.
35. Otting, G., Liepinsh, E., and Wuthrich, K. (1993) *Biochemistry 32*, 3571−3582.
36. Czapinska, H., Otlewski, J., Krzywda, S., Sheldrick, G. M., and Jaskolski, M. (2000) *J. Mol. Biol. 295*, 1237−1249.
37. Oldfield, E. (1995) *J. Biomol. NMR 5*, 217−225.
38. Spera, S., and Bax, A. (1991) *J. Am. Chem. Soc. 113*, 5490−5492.
39. Blanchard, L., Hunter, C. N., and Williamson, M. P. (1997) *J. Biomol. NMR 9*, 389−395.
40. Baxter, N. J., and Williamson, M. P. (1997) *J. Biomol. NMR 9*, 359−369.
41. Anderson, A. G., and Hermans, J. (1988) *Proteins 3*, 262−265.
42. Beeser, S. A., Oas, T. G., and Goldenberg, D. P. (1998) *J. Mol. Biol. 284*, 1581−1596.
43. Kim, K.-S. (1991) in *Biochemistry*, pp 196, University of Minnesota, St. Paul, MN.
44. Tüchsen, E., and Woodward, C. (1987) *Biochemistry 26*, 8073−8078.

BI011693E